Journal of CO2 Utilization 51 (2021) 101655

Contents lists available at ScienceDirect

Journal of CO2 Utilization

journal homepage: www.elsevier.com/locate/jcou

Post-combustion carbon capture for tank to propeller via process modeling and simulation

Chenxi Ji [a,b], Shuai Yuan [a], Mitchell Huffman [a], Mahmoud M. El-Halwagi [a,b], Qingsheng Wang [a,*]

[a] Mary Kay O'Connor Process Safety Center, Artie McFerrin Department of Chemical Engineering, Texas A&M University, College Station, TX, 77843, United States
[b] Gas & Fuels Research Center, Artie McFerrin Department of Chemical Engineering, Texas A&M University, College Station, TX, 77843, United States

ARTICLE INFO

Keywords:
Tank to propeller
Post-combustion carbon capture
Maritime carbon capture
MDEA-PZ solvent
Process modeling

ABSTRACT

The International Maritime Organization (IMO) has issued a long-term sustainable strategy to gradually phase out the major ship-related sources of greenhouse gas emissions. While the post-combustion carbon capture has been well investigated for onshore plants, the maritime carbon capture system is still in an early stage due to its unique characteristics and design limitations. Aiming at providing a holistic way to find the most efficient and sustainable PCC solution for an LNG tanker, this work proposed a system of the tank to propeller post-combustion carbon capture which integrates ship engine process modeling with chemical absorption/desorption process modeling techniques. A rate-based aqueous monoethanolamine (MEA) process model was developed and validated, then scaled up and modified to capture CO_2 from the flue gas. To increase the carbon capture efficiency and decrease the energy penalty, this work provided detailed steps for process model development covering innovative absorber/stripper design under variation of solvents, packed type, and liquid to gas ratio. This work also included a thorough sustainability evaluation based on emission reduction efficiency, energy penalty, and carbon cyclic capacity among two single aqueous amines, MEA and diisopropanolamine (DIPA), and one blended amine with a promoter, methyldiethanolamine (MDEA) with piperazine (PZ). Although DIPA presented a better performance on energy requirement for solvent regeneration, the blended amine was the optimal solvent to meet the requirement of the IMO carbon abatement strategy. Compared to the seven molality MEA, the MDEA-PZ option could capture more than 57 % CO_2 while around 25 % specific reboiler duty can be saved.

1. Introduction

Greenhouse gas emission has been bringing great concerns into the public for decades. In the shipping industry, the Marine Environment Protection Committee (MEPC) of the International Maritime Organization (IMO) has issued a long-term plan to phase out the major ship-resulted air polluters, such as SO_x, NO_x, and CO_2. Carbon emissions are set to be reduced by at least 40 % by 2030 and 70 % by 2050 compared to the benchmark emissions of 2008 [1].

A typical shipping fuel value chain typically involves the stages of feedstock extraction, shipping fuel production, logistic support (including transportation, storage, and distribution), and fuel use. Emissions are associated with every stage of the shipping fuel value chain. A wide agreement has been reached in the field of life cycle assessment to integrate the first three upstream stages into one process: well to tank (WTT) process, and the stage of fuel combustion and use on board is called tank to propeller (TTP) process. Fig. 1 shows grams CO_2 equivalent (CO_2, CH_4 and N_2O considered) per megajoules of energy contained in heavy fuel oil (HFO) (g CO_2eq/MJ) of the WTT and TTP from our collected data [2–10]. The median value of the TTP CO_2 equivalent emissions is 78 g per MJ while that value of WTP is around 10 g per MJ. Therefore, the TTP carbon capture is essential for the global warming effects of the whole shipping fuel supply chain.

Common practice of maritime CO_2 emission reduction encompasses the optimal design of propulsion system [11,12], cleaner and safer shipping fuels substitution [13,14], maritime carbon capture and storage [15,16] and thermal efficiency improvement via onboard waste heat recovery [17,18]. Unlike the widely investigated carbon capture studies for onshore facilities, research on maritime/onboard carbon capture is still in an early stage: it was firstly proposed by Det Norske Veritas (DNV) and Process Systems Enterprise (PSE) in 2013 [19], and only limited publications have focused on this area since. As one specific type of combustion carbon capture, the maritime carbon capture techniques can be classified as:

* Corresponding author.
E-mail address: qwang@tamu.edu (Q. Wang).

https://doi.org/10.1016/j.jcou.2021.101655
Received 19 April 2021; Received in revised form 15 June 2021; Accepted 15 July 2021
Available online 20 July 2021

- Pre-combustion capture: carbon is separated from H_2, H_2 is used for combustion
- Oxy-fuel combustion: air for combustion is replaced by pure O_2, then CO_2 and H_2O are separated
- Post-combustion capture: CO_2 is removed from flue gases produced during the combustion of fuels using air

When considering technology maturity, the post-combustion carbon capture is the most favorable one to apply for the tank to propeller process. In particular, the tank to propeller post-combustion capture approaches may involve adsorption, cryogenic carbon capture, solvent-based chemical absorption, physical absorption and membrane-based technologies. Fig. 2 (a) shows the simplified process flow diagram of solvent-based chemical absorption-type tank to propeller post-combustion carbon capture (TTPPCC), while Fig. 2 (b) illustrates the major process units and the available solvent options of the TTPPCC process. The fuel tank continuously sends the shipping fuel to the ship main engine. Both the shaft work and flue gas are generated by the fuel combustion in the engine chamber. While the effective work constantly provides axial thrust to the propeller to move the ship, the produced flue gas is processed by the post-combustion carbon capture system. The flue gas firstly reacts with the lean solvent solution in the absorber, leaving the treated gas with a lower CO_2 content. Then the rich solvent (high CO_2 stream) is desorbed in the stripper, the top of which is connected to the compressed CO_2 tank for storage. The regenerated solution passes through a heat exchanger for heat recovery and goes back to the absorber.

Since marine vessels have limitations of space and utilities, the TTPPCC system design should take into account the dimensions of the absorber and stripper and the supply of heat and electric power. In addition, the reaction kinetics and carbon capture equipment stability must be carefully considered as the tank to propeller CO_2 capture operation is in a constantly moving environment. The first work on maritime post-combustion carbon capture in public domain was presented by Luo et al. [15], who employed process simulation for one cargo ship under three scenarios, one without carbon capture as a reference case and the other two cases with either monoethanolamine (MEA) based PCC or MEA solvent with an additional diesel gas turbine. In 2019, Feenstra et al. [16] used two solvent options,30 wt% aqueous MEA and 30 wt% aqueous piperazine (PZ), for two ships with both diesel and LNG engines. Utilizing Luo and Wang's ship engine model [15], Awoyomi [20] applied 3.5 % and 4.1 % ammonia to capture CO_2 and SO_2 simultaneously to meet the requirements of both the IMO 2020 sulfur cap and 2030 IMO CO_2 strategy. Another aspect should be noticed in the process design stage is that the CO_2 concentration in the flue gas shares different values from a power plant compared to a TTPPCC system. Before entering into the carbon capture system, the flue gas from an onshore power plant contains 12−15 mol% CO_2 [21], while the typical CO_2 mole fraction in the ship-based flue gas is around 4−7 mol% [15,16,20]. The lower CO_2 concentration at the TTPPCC system inlet requires a rigorous regime to screen solvent options and solvent concentration to achieve the target carbon capture rate of 90 %. This study finalized three solvent options (MEA, DIPA, and MDEA with PZ) with specific concentration by considering solvent solubility, absorption rate, reaction rate, and thermal degradation.

This manuscript aims at providing a holistic way to determine the most efficient and sustainable post-combustion carbon capture solution for tank to propeller processes. The objectives of this work encompass the following: 1) marine engine cylinder modeling and validation, 2) TTPPCC system process model development and pilot plant validation, 3) Optimal absorber and stripper design under variation of solvents, packed type and liquid gas ratio, 4) Quantitative sustainable evaluation by emission reduction efficiency, energy penalty and carbon cyclic capacity.

Our previous study [22] focused on the emission estimation under the current IMO sulfur cap among multiple ship types and emissions sources. As a follow up study, this manuscript will provide the most effective way to contain ship-resulted carbon volume via process intensification techniques. To the best knowledge of the authors, this paper firstly explored a thorough sustainable performance analysis of a TTPPCC system by employing process modeling methodology. Also, this is the first time a maritime post-combustion carbon capture system has been modeled using a blended amine with PZ as a promoter.

2. Maritime system design

For decades, the larger-scale ship has displayed a great potential for improved fuel efficiency and emission control per unit of cargo, as well as a good return on investment. There is a clear trend of embracing the era of larger-scale ships. However, no study has focused on simulation of the carbon capture system for larger sized ships. The size of the reference ships for the maritime PCC studies are in a surprisingly small range, with a maximum displacement of 20,550 cubic meters for an LPG tanker [20]. Moreover, the ship engine is another perspective to consider in the sustainable maritime solution. The two-stroke slow speed diesel engine still dominates the ship engine market, while many dual-fuel engine options (mainly marine diesel fuel and LNG) are available to meet the current IMO emission standard. Based on our collected data, no study in the maritime carbon capture field has focused on process modelling for the 2-stroke dual-fuel engine type. As a milestone study in the maritime post-combustion carbon capture, Luo and Wang [15] established the process model for a two-diesel-engine power system, while most other

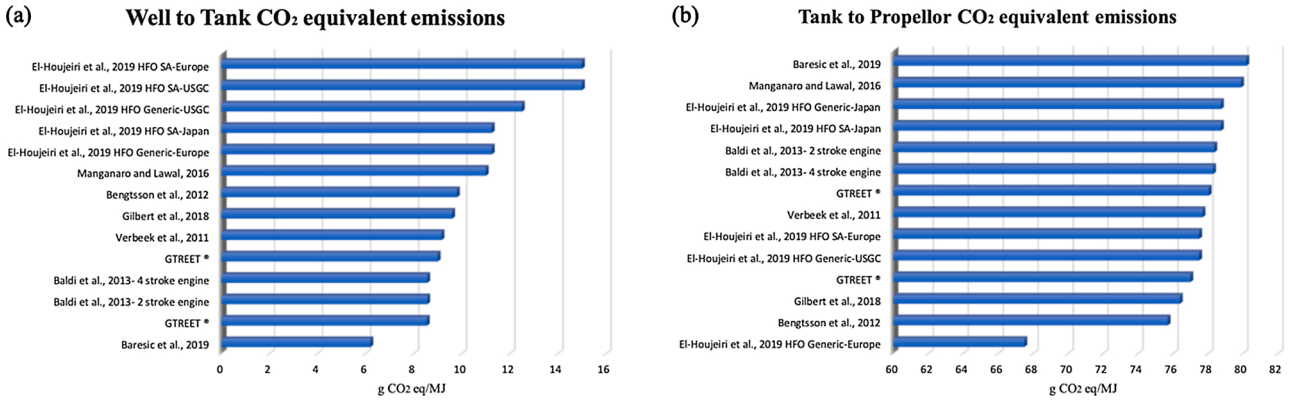

Fig. 1. CO_2 equivalent emission for well to tank (1a) and tank to propeller(1b) processes.

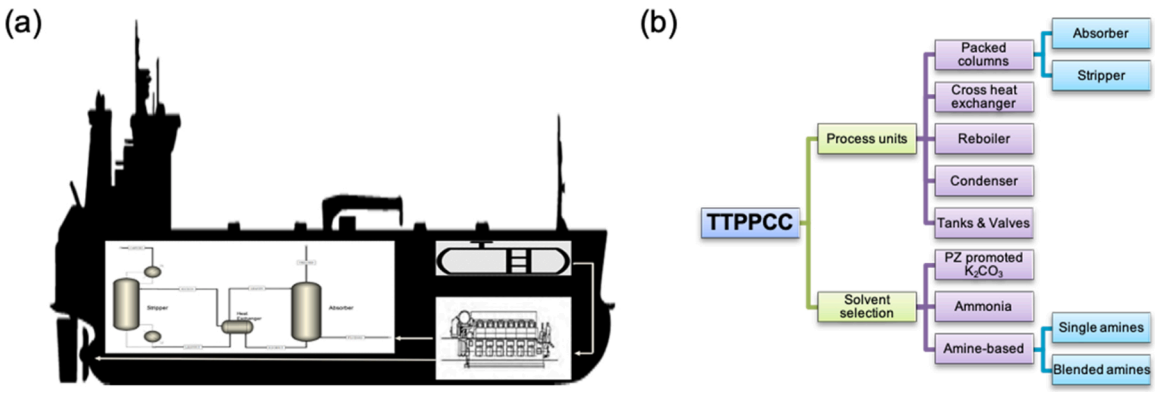

Fig. 2. (a) Simplified process flow diagram of TTPPCC; (b) Major process units and solvent options of TTPPCC.

studies pay more attention to modeling the single-diesel main engine.

2.1. Reference LNG tanker

Three strategies of sulfur emission control including ship exhaust gas scrubber, oil change to the low sulfur shipping fuels, and engine change to LNG-driven type are currently available for ship owners under IMO 2020 sulfur cap. When considering long-term carbon emission reduction, the LNG-fueled engine is the most attractive option. Therefore, the study targeted the LNG dual-fuel engine to establish the modeling of the tanker to propeller process. Tab. S-1 in the supplemental document lists the parameters of the reference LNG tanker [23], which used to be the largest LNG carrier before the Q-flex and Q-max era. The ship can be driven by either marine diesel fuel or LNG with three V-type dual engines and one L-type dual engine [23]. The fuel consumed in the LNG tanker is set as the marine diesel oil and its inherent properties are listed in Table 1.

2.2. Tank to propeller process model development

The tank to propeller process of the targeted ship was modeled by Aspen Plus V11. At the property stage, the airflow (mainly nitrogen and oxygen) and marine diesel oil flow (see Table 2) were input using the Peng-Robinson equation of state as the property method with Boston-Mathias modifications. The TTP process in the simulation stage has four functional modules: compression module, fuel combustion module, mixing module, and integration module. The block models of *Compr, RGibbs, Mixer,* and *Hierarchy* were employed for the four modules, respectively.

Referenced from the manual book of Wärtsilä 12V50DF and 6L50DF [23], the input value of fuel flow and airflow can be calculated accordingly, as well as the shipping fuel temperature and mean effective pressure in the engine cylinder. Fig. 3 (a) shows the tank to propeller flow chart of 12V50DF. The fresh air is preprocessed by filter, compressor, and cooler before it is mixed and reacted with injected marine diesel fuel in the engine cylinder, then one part of the high-temperature exhaust gas is cooled down and another part is entering the turbocharger. Using a similar theory, the model of 6L50DF is built as shown in Fig. 3 (b). The detailed process models for the two dual engines can be found in the Fig. S-1 of the supplemental materials. The 4-engine ship power system is integrated by four *Hierarchy* blocks, displayed in Fig. 3 (c). The effective work is then sent to the propeller and the total exhaust gas enters the post-combustion carbon capture system.

To validate the proposed TTP process model, the simulated results for the two engines (see Tab. S-2 from the supplemental document for details) are compared with the data abstracted from the Wärtsilä 50DF product guidebook. The validation results displayed in Table 2 present

Table 1
Inherent properties for marine diesel oil [24].

Types	Name	LHV (MJ/kg)	Density (g/cm3)	RON	Weight %
Branched alkanes	Iso-cetane/ HMN	44.38	0.321	98.9	0.1786
Aromatic HCs	1-Methylnaphthalene	40.27	0.548	120	0.1776
Naphthenic HCs	Decalin	43.02	0.569	46	0.36
N-alkanes	N-hexadecane	45.23	0.268	−30	0.2838

Table 2
Marine engine cylinder process simulation output and validation.

Engine Type	Load	SFOC (kg/s)	Comp. Air Flow Rate (kg/s)	Validation	Engine Output (kw)	Ex. Gas Flow Rate (kg/s)
12V50DF	100	0.62	21.9	Manual	11700	23.8
				Model	11623	22.52
				Prediction Dev. (%)	−0.66	−5.38
	85	0.604	18.61	Manual	9945	19.7
				Model	9877	19.22
				Prediction Dev. (%)	−0.68	−2.44
	75	0.599	16.42	Manual	8775	18.2
				Model	8714	17.02
				Prediction Dev. (%)	−0.69	−6.48
	50	0.618	11.9	Manual	5850	13.9
				Model	6315	12.52
				Prediction Dev. (%)	7.94	−9.92
6L50DF	100	0.308	11.0	Manual	5850	12.4
				Model	5838	11.31
				Prediction Dev. (%)	−0.21	−8.79
	85	0.302	9.35	Manual	4972	10.1
				Model	4962	9.66
				Prediction Dev. (%)	−0.20	−4.36
	75	0.3	8.25	Manual	4387	9.2
				Model	4378	8.55
				Prediction Dev. (%)	−0.21	−7.06
	50	0.309	6.0	Manual	2925	7.1
				Model	3184	6.4
				Prediction Dev. (%)	8.96	−9.85

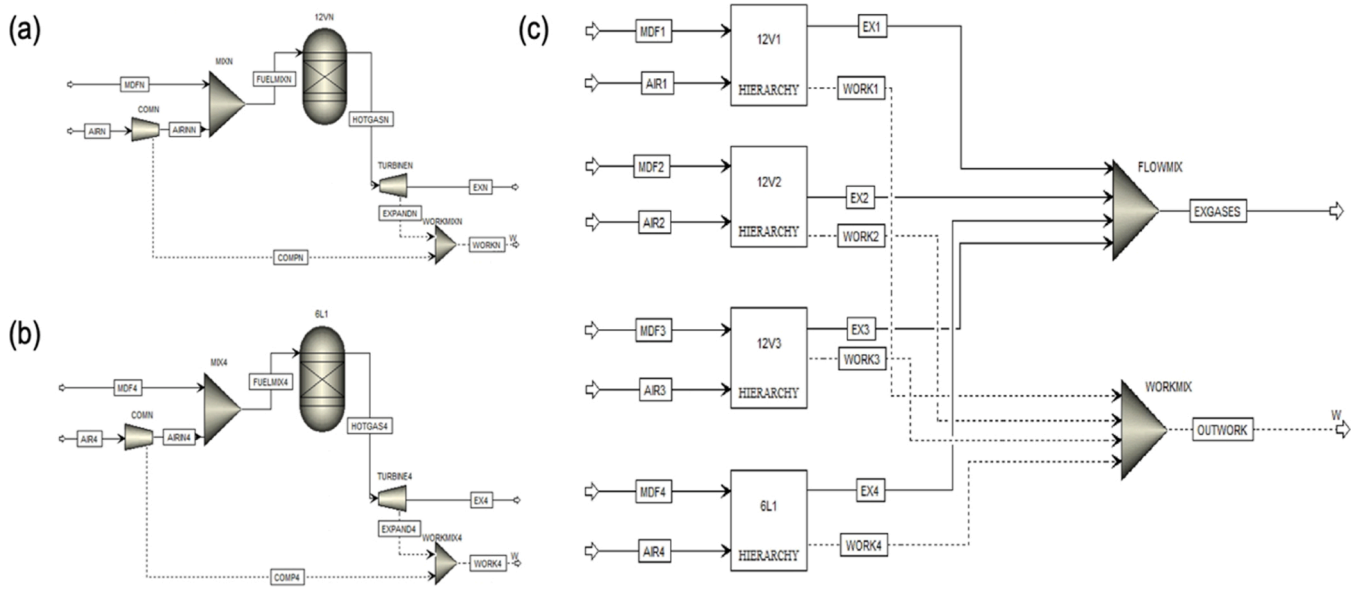

Fig. 3. Process flow charts for two types of marine engines: a) 12V50DF; b) 6L50DF; c) Simplified process modeling for the target ship engine system.

good agreement for the values of the simulated engine output power and exhaust gas flow rate across all load levels. The maximum prediction deviation for the V-type engine is -9.92 % at 50 % load level, while that for the L-type is -9.85 % at 50 % as well. 85 % workload simulation outputs will be applied to the following TTPPCC system process modeling since it is a common practice to assume 85 % engine load when the ship is in the navigation mode.

3. TTPPCC process model development

Extensive studies have focused on the only commercialized CO_2 capture technology, post-combustion carbon capture system. For ships powered by fossil fuels, the solvent based TTPPCC methodology is the most promising process for implementing this technology. Many previous milestone works in the field of PCC have pointed out the MEA as an ideal solution for carbon capture because of its high CO_2 solubility, acceptable reaction kinetics, and fair price. In this manuscript, the MEA with molality of 7 m (30 % in weight percent) was employed to establish the base case process model for the TTPPCC system. Furthermore, the unique features and operation limitations of TTPPCC have been identified and shown in Table 3, and the corresponding process modeling considerations are listed as well.

Based on Table 3, the major considerations to improve the performance of the TTPPCC process with a maritime process intensification study are: the optimized dimension of process units, variant lean solution flows, and intensified absorption/desorption reactions with the least negative effects.

3.1. Physical solubility and Henry's constant

Using the same approach of molecular interaction calculations as the electrolyte NRTL, the eNRTL- Redlich-Kwong (RK) property method is applicable for handling aqueous and mixed solvent systems with a wide range of concentrations [25]. This work adopted eNRTL-RK equation of state (EOS) to compute the liquid phase thermodynamic properties, while the PC-SAFT was utilized for vapor property calculations of the MEA-H_2O-CO_2 system. The Henry's constant of the mixture is calculated from the binary Henry's constants of pure solvents (see Eq. 1):

$$\ln\left(\frac{H_i}{\gamma_i^{\infty}}\right) = \sum_A w_A \ln\left(\frac{H_{iA}}{\gamma_{iA}^{\infty}}\right) \quad (1)$$

where H_i is Henry's constant for binary components, γ_i^{∞} is the infinite dilution activity coefficient of molecular solute i in the mixed solvent, H_{iA} Henry's constant of molecular solute i in pure solvent A, γ_{iA}^{∞} is the infinite dilution activity coefficient of molecular solute i in pure solvent A. w_A, the weighting factor, is calculated by Eq. 2:

Table 3
Features, limitations and modelling considerations of TTPPCC.

Features of TTP	Limitations of TTPPCC	TTPPCC modelling considerations
Limited space	Size/ height of equipment	Constraints in absorber/ stripper dimension determination
Limited utilities	Supply of heat, electric power, *etc.*	Energy penalty/ Required regeneration energy
Long lasting constant movement	Fast reaction rate, Equipment effectiveness & stability	Solvent selection preference: stable, fast reaction kinetics, not subject to degradation
Multiple operation modes	Integrated carbon capture stategies	Scenario based process models, variant of L/G ratio
Vulnerable marine environment	Toxic/high corrosive substance release	Low toxic & corrosive solvent preferred, packed materials with high packing factor preferred

Table 4
Correlation coefficients of Henry's law constants.

Binary components	CO_2-H_2O	CO_2-MEA	N_2- H_2O	O_2-H_2O	H_2S-H_2O
Source	Yan and Chen [27]	Liu et al. [28]	APV Binary [29]	APV Binary [29]	APV ENRTL-RK [29]
Unit	N/sqm	N/sqm	N/sqm	N/sqm	N/sqm
T	273–473 *K*	280–600 *K*	273–346 *K*	274–348 *K*	273–423 *K*
C1	100.65	89.452	176.507	155.921	358.138
C2	−6147.7	−2934.6	−8432.77	−7775.06	−13236.8
C3	−10.191	−11.59	−21.558	−18.3974	−55.0551
C4	0	0.001644	−0.008436	−0.009444	0.05957

$$w_A = \frac{x_A (V_{iA}^{\infty})^{2/3}}{\sum_B x_B (V_{iB}^{\infty})^{2/3}} \quad (2)$$

where x_A is the mole fraction of solvent A on solute-free basis, V_{iA}^{∞} is the partial molar

volume of molecular solute i at infinite dilution in pure solvent A and its calculation process is referred to as the Brelvi-O'Connell model [26]. Henry's law constants H_{i_1, i_2} of the binary components (i_1, i_2) in this study follow the below equation:

$$H_{i_1, i_2} = \exp\left(C_1 + \frac{C_2}{T} + C_3 lnT + C_4 T\right) \quad (3)$$

where C_1, C_2, C_3, C_4 are the correlations for binary Henry's law constants, and T is the system temperature. Table 4 displays the correlation coefficients for the determination of Henry's law constants on a molality basis. This study adopted the model of Yan and Chen [27] to calculate the Henry's constant of CO_2 and H_2O, and CO_2-MEA was extracted from the work of Liu et al. [28]. The correlation coefficients of N_2- H_2O and O_2-H_2O were both from the APV Binary database, while the APV ENRTL-RK database was applied for the H_2S-H_2O binary pair. The default values from the Aspen Databank were used for other Henry's constants of the binary components [29].

3.2. Carbon capture chemical reaction mechanism

The equilibrium reactions and kinetics-Controlled reactions of the MEA-CO_2-H_2O mixture have been well investigated, and Table 5 summarizes the two categories of the aqueous phase chemical reactions in this work.

The equilibrium constants (K_i) for reactions 1–5 in MEA were calculated from the reference state Gibbs free energies of the participating components by Eq. 4 [30]:

$$-RTlnK_p = \Delta G_p^{\circ} \quad (4)$$

where R is the universal gas constant, T is the system temperature, K_p is the chemical equilibrium constant of reaction p, and ΔG_p° is the reference state Gibbs energy change for reaction p. The kinetics-controlled reactions (6–9 in Table 5) are governed by the power law expressions expressed in the below equation:

$$r_q = k_q^{\circ} T^n \exp\left(-\frac{E_q}{RT}\right) \prod_{i=1}^{N} (x_i \gamma_i)^{\varepsilon_{iq}} \quad (5)$$

where r_q is the reaction rate for reaction q, k_q° is the pre-exponential factor, T^n is the system temperature with temperature factor n, E_q is the activation energy, R is the gas constant, x_i is the molar fraction of component i, γ_i is the activity coefficient of component i, and ε_{iq} is the stoichiometric of component i in reaction q.

The rate-based mass transfer correlations can be found in the Tab. S-3 of the supplemental document, and the parameters of the other components were collected from the databank of Aspen Plus [29].

Table 5
Reactions in the kinetic model for MEA-CO_2-H_2O system.

Reaction No.	Reaction Type	Stoichiometry
1	Equilibrium	$MEAH^+ + H_2O \leftrightarrow H_3O^+ + MEA$
2	Equilibrium	$2H_2O \leftrightarrow H_3O^+ + OH^-$
3	Equilibrium	$HCO_3^- + H_2O \leftrightarrow H_3O^+ + CO_3^{2-}$
4	Equilibrium	$H_2S + H_2O \leftrightarrow HS^- + H_3O^+$
5	Equilibrium	$H_2O + HS^- \leftrightarrow S^{2-} + H_3O^+$
6	Kinetic	$CO_2 + OH^- \rightarrow HCO_3^-$
7	Kinetic	$HCO_3^- \rightarrow CO_2 + OH^-$
8	Kinetic	$MEA + H_2O + CO_2 \rightarrow MEACOO^- + H_3O^+$
9	Kinetic	$MEACOO^- + H_3O^+ \rightarrow MEA + H_2O + CO_2$

3.3. Base case design and validation

Fig. 4 shows the base case process model of TTPPCC with the major columns of absorber and stripper. Two water makeup streams (one for the pre-cooling module and another for the absorption module) and one MEA replenishment before the *leanin* flow were incorporated in the PCC process, and the operation conditions of the pilot plant were extracted from experiment 1 of the Notz study to validate the proposed TTPPCC model. The key parameters of TTPPCC validation were identified as Leanin/Richout flow CO_2 loading, CO_2 emission reduction efficiency (CRE), captured CO_2 flow rate, and reboiler or specific reboiler duty. In particular, the Leanin/Richout flows are expressed per amount of CO_2 absorbed, the CRL is calculated from the CO_2 mass difference between the flue gas and the exhausted gas, and the captured CO_2 is the amount of CO_2 regenerated after the desorption operation. The energy required by the reboiler was determined by the sum of the latent heat water condensation (Q_{cond}), the sensible heat for solvent to reach reboiler temperature (Q_{sh}) and the heat of CO_2 desorption (Q_{des}), then the penalty energy is calculated by integrating the reboiler duty and the captured CO_2 flow rate. The equations of the validation parameters are represented below:

$$\alpha_{leanin\ (richout)} = \frac{[CO_2] + [HCO_3^-] + [CO_3^{2-}] + [MEACOO^-]}{[MEA] + [MEAH^+] + [MEACOO^-]} \quad (6)$$

$$CRE = \frac{y_{co_2,FG} \bullet F_{FG} - y_{co_2,EG} \bullet F_{EG}}{y_{co_2,FG} \bullet F_{FG}} \quad (7)$$

$$Q_{reb} = Q_{cond} + Q_{sh} + Q_{des} = m_w \Delta H_w + m_s c_p (T_{bottom} - T_{top}) - m_{co_2} \Delta H_{co_2} \quad (8)$$

$$Q_{spe}\left(\frac{MJ}{kg}\ CO_2\right) = \frac{Q_{reb}}{F_{cap\ CO_2}} \quad (9)$$

The experimental data of the pilot plant (Mellapak 250Y packing type) were extracted from the case 1 of Notz et al.'s study [31]. The method from Bravo's research group [32] was applied to determine corrections for the mass transfer coefficients and effective interfacial area on the liquid and gas side. The results of the flows of *leanin, richout, gasout,* and *co2out*, and the reboiler duty value was obtained by the proposed model. Employing Eq. 6–9, the validation results were calculated and summarized in Table 6. The largest absolute relative deviation of 7.9 % is located in the specific reboiler duty, and others are consistent with the experimental data as well, leading to the conclusion that the proposed model appears to be in line with experimental results. Moreover, the validation process for Sulzer BX, Mellapak plus 252Y, and Flexipac 2Y were completed with acceptable results as well, see Table S-4 in the supplemental document for details.

4. TTPPCC process simulation and performance analysis

After the process synthesis, design, and analysis, the well-known MEA-based PCC operation has been set as the base case of the TTPPCC model with good validation results. As per the framework of the sustainable process synthesis-intensification [33], the innovation design should be the next focus to find a more eco-friendly solution for our defined maritime system. Referenced from the above-mentioned considerations in Table 3 of TTPPCC modelling, the alternative design for intensified unit operations would involve sustainable solvent selection, optimal column dimension determination, variance of L/G ratio, and minimal energy penalty for the TTPPCC system.

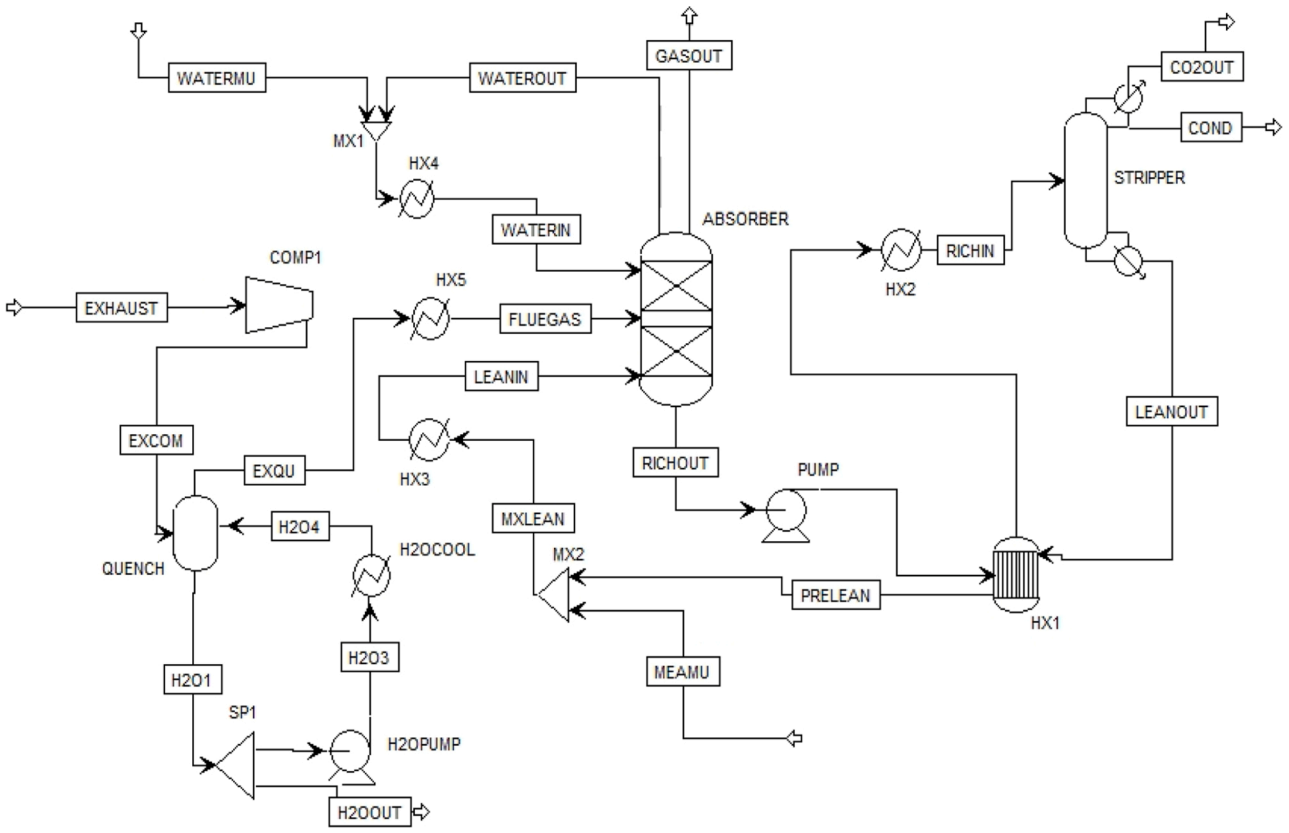

Fig. 4. Base case design of the TTPPCC process.

Table 6
Pilot plant carbon capture process simulation outputs and validation.

Variable	Experiment output [31]	Rate-based model output	Absolute relative deviation, %
Lean in CO_2 loading (mol CO_2/mol MEA)	0.265	0.273	3.0
Rich out CO_2 loading (mol CO_2/mol MEA)	0.386	0.386	0
CO_2 emission reduction efficiency (%)	76.0 %	73.9 %	2.7
Captured CO_2 rate (kg/h)	4.65	4.51	3.0
Reboiler duty (kw)	6.48	6.80	4.9
Specific reboiler duty (MJ/kg CO_2)	5.02	5.42	7.9

Table 7
Major input values of MEA -based maritime PCC.

Entering gas	Flow rate (kg/s)	67.32
	Average molecular weight (g/mol)	28.91
	Temperature (℃)	48
	Pressure (bar)	1
	Density (kg/m^3)	1.089
Entering solvent	Flow rate (kg/s)	67.32/134.64/201.96/269.28
	Temperature (℃)	40
	Density (kg/m^3)	1053.39
	Viscosity at 40 ℃ (cP)	3

4.1. Intensified TTPPCC design

Following the 7 m MEA case, the alteration process design is processed with varying inputs of *leanin* flow rates and different structured packed types to find the optimal L/G ratio and design diameter of the absorber under acceptable flooding percentage, which is assumed to be 80 % in this work.

In the contribution of Agbonghae et al. [34], the range of L/G (kg/kg) ratio is from 0.70 to 2.75 for gas-fired power plants and is from 2.00 to 5.50 for coal-fired power plants. This study selected the point values 1 to 4 as the variant L/G ratio to conduct the calculation of column diameter of different structured packed types, involving BX, Mellapak plus 252Y, Mellapak 250Y and Flexipac 2Y.

The packed column parameters such as liquid/gas (L/G) ratio, diameter, packed height and total height were determined using physical modeling with two–film gas–liquid absorption theory. The input values of MEA-based on-board PCC are displayed in Table 7.

For the absorber design, the recommended value of liquid pressure drop is between 15–50 mm H_2O per meter packed area [36]. This study assumed the drop line of 20.83 mmH_2O per meter packing for the present design of absorber and stripper. Fig. 5 shows the generalized pressure drop correlation [35], the relationship between flooding correlation factor (K_4) and the flow parameter (F_{LV}), and their equations are listed below:

$$F_{LV} = \frac{L}{G}\sqrt{\frac{\rho_V}{\rho_L}} \tag{10}$$

$$K_4 = \frac{13 \bullet \left(V_w^*\right)^2 F_p \left(\frac{\mu_L}{\rho_L}\right)^{0.1}}{\rho_v(\rho_L - \rho_v)} \tag{11}$$

where V_w^* is the gas mass flow rate per unit column cross-sectional area,

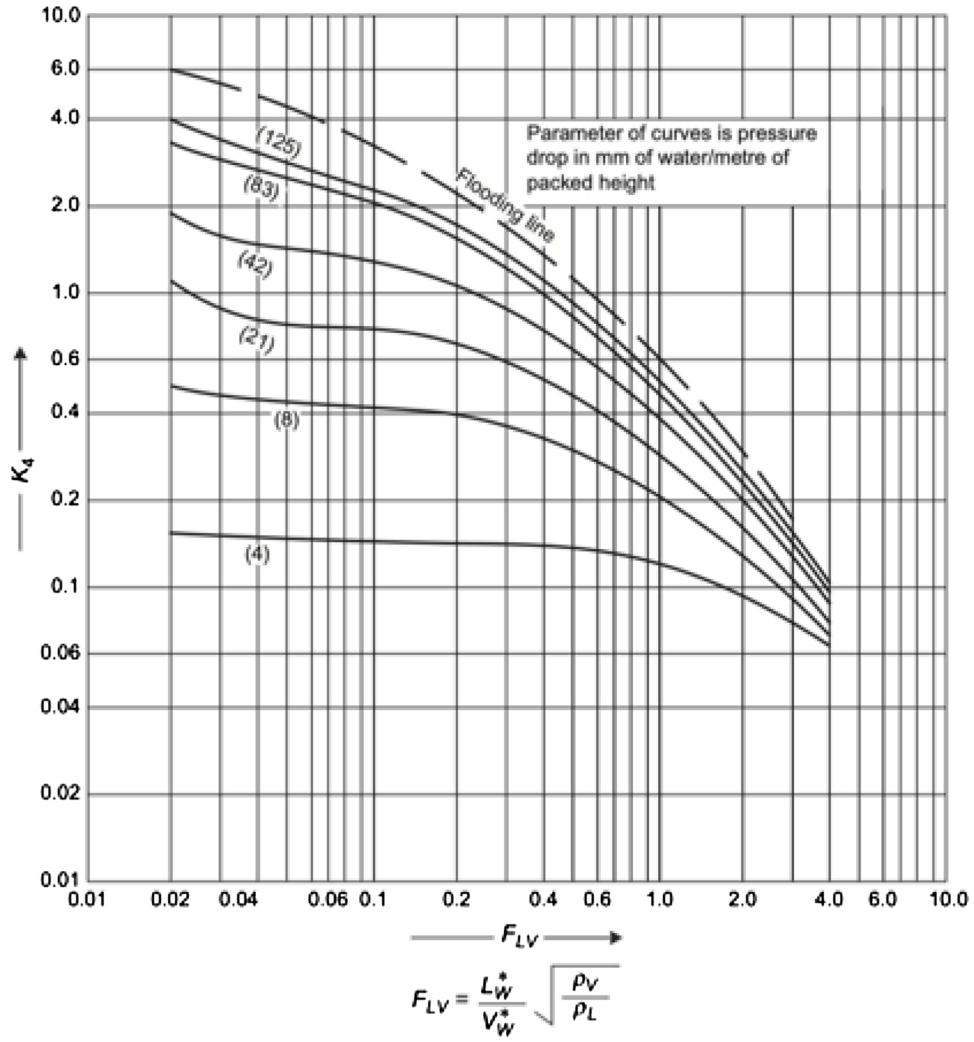

Fig. 5. Generalized pressure drop correlation [35].

F_p is the packing factor, μ_L is the liquid viscosity, ρ_L and ρ_v are the liquid density and vapor density, respectively.

Besides the flooding correlation factor (K_4), its corresponding flooding factor (K_{fl}) can also be found from Fig. 5, and the column flooding percentage (CFP) is calculated by:

$$CFP = \sqrt{\frac{K_4}{K_{fl}}} \tag{12}$$

After the V_w^* is calculated, the trial cross-sectional area and trial diameter can be determined. The designed diameter and cross-sectional area for varying L/G ratio and multiple packing types are shown in Table 8.

4.2. Analysis of solvent selection

Due to the unique features of maritime PCC (see Table 3), the criteria of solvent selection are as follows: fast kinetics, minimal energy penalty, less prone to degradation, less corrosive, and neglectable toxicity. In addition, to reduce the sensible heat loss and the dimension of maritime PCC system, the solvent should have high cyclic capacity, which refers to the difference between the CO_2concentration in the rich and lean solution. The molar cyclic CO_2 absorption capacity (the cyclic capacity in this work) of aqueous single and blended amines is defined as:

$$\Delta\alpha = \alpha_{richout} - \alpha_{leanin} \tag{13}$$

where α_{leanin} represents the CO_2loading of the initial amine solution, and $\alpha_{richout}$ is the CO_2loading of the amine solution after absorption.

One single aqueous amine and one blended amine were selected to find an optimal solution of the proposed TTPPCC system. Diisopropanolamine (DIPA) was chosen as the single amine for the TTPPCC system since the aqueous DIPA solution requires less energy to regenerate, removes CO_2 without degradation of the solution, and also is less corrosive and has greater selectivity of H_2S toward CO_2 [37]. Moreover, the methyldiethanolamine (MDEA) is another alkanol-amine which has less regeneration cost, lower volatility, greater thermal stability and higher CO_2 cyclic capacity. However, both DIPA and MDEA have one common weakness for maritime carbon capture, a lower second order CO_2 absorption rate constant (K_2) than MEA [38], leading to their inferior absorption reaction rate. Many studies have pointed out the blended amine with the promotor PZ is a superior solution to resist to degradation with higher kinetic rates. Therefore, this study proposed an intensified maritime carbon capture process using a MDEA-PZ-CO_2-H_2O system.

This study completed 40 process simulations in total: 16 groups for MEA, 16 groups for DIPA, and 8 groups for MDEA-PZ (since the flooding percentage of absorber and stripper exceeded 80 % when L/G ratio was set as 3 and 4). The input values of selected variables for the TTPPCC system, including the composition of the selected solvent in *leanin* flow, the calculated *richout* loading range, and the diameter, stages and height of absorber and stripper, are listed in Table 9. Unlike the PCC system of

Table 8
The designed diameter and cross-sectional area for variant L/G ratio and multiple packing types.

Liquid gas ratio	Flow para., F_{LV}	Flooding corr. factor, k_4	Packed type	Packing factor (m-1), F_p	Gas mass flowrate per unit column C/S area (kg/m2s), V_w^*	Trial C/S area (m^2), a	Trial diameter (m), d	Flooding factor, K_{fl}	Trial flooding percentage (%)	Design diameter (m)	Column C/S area (m^2)	Column flooding percentage (%)
1.0	0.032	0.90	Mellapak plus 252Y	39.0	2.701	24.927	5.635	5.4	0.408	6.0	19.63	0.518
			Flexipac 2Y	49.0	2.409	27.941	5.966			6.0	23.76	0.480
			Mellapak 250 Y	66.0	2.076	32.427	6.427			6.5	28.27	0.468
			Sulzer BX	90.0	1.778	37.867	6.945			7.0	33.18	0.466
2.0	0.064	0.80	Mellapak plus 252Y	39.0	2.546	26.439	5.803	4.0	0.447	6.0	19.63	0.602
			Flexipac 2Y	49.0	2.272	29.635	6.144			6.5	23.76	0.558
			Mellapak 250 Y	66.0	1.957	34.394	6.619			7.0	28.27	0.544
			Sulzer BX	90.0	1.676	40.164	7.153			7.5	33.18	0.541
3.0	0.096	0.78	Mellapak plus 252Y	39.0	2.514	26.776	5.840	3.4	0.479	6.0	23.76	0.540
			Flexipac 2Y	49.0	2.243	30.013	6.183			6.5	23.76	0.605
			Mellapak 250 Y	66.0	1.933	34.832	6.661			7.0	28.27	0.590
			Sulzer BX	90.0	1.655	40.675	7.198			7.5	33.18	0.587
4.0	0.129	0.70	Mellapak plus 252Y	39.0	2.382	28.265	6.000	3.1	0.475	6.5	23.76	0.565
			Flexipac 2Y	49.0	2.125	31.682	6.353			6.5	28.27	0.533
			Mellapak 250 Y	66.0	1.831	36.769	6.844			7.0	28.27	0.618
			Sulzer BX	90.0	1.568	42.937	7.396			7.5	33.18	0.615

Table 9
TTPPCC process simulation input variables.

	Solvent		
Input variables	MEA	DIPA	MDEA-PZ
Composition (on molality scale)	7 m	6 m	5 m + 5 m
Leanin loading (mole CO_2/mole amine)	0.199	0.029	0.127
Richout loading range (mole CO_2/mole amine)	[0.309, 0.489]	[0.195, 0.318]	[0.406, 0.489]
Diameter of absorber (stripper)	BX: 7.5(4.5) M 250: 7 (4.5) Mp 252: 6.5 (4.5) 2Y: 6.5(4.5)	BX: 7.5(4.5) M 250: 7 (4.5) Mp 252: 6.5 (4.5) 2Y: 6.5(4.5)	BX: 7.5(6.5) M 250: 7 (6.5) Mp 252: 6.5 (6.5) 2Y: 6.5(6.5)
Stages of absorber (stripper)	20 (8)	20 (8)	20 (8)
Height of absorber (stripper)	10 (6)	10 (6)	10 (6)

onshore facilities, the limited space (particularly the height of columns) on the ship should be a solid constraint for TTPPCC system design rather than setting the 90 % carbon capture amount as the abatement goal.

4.3. TTPPCC system performance analysis

The black dashed line and orange dashed line in Fig. 6 represent IMO 2030 and 2050 carbon reduction goals, respectively. In general, the MEA outperforms DIPA in every defined scenario. There is a clear trend that the carbon reduction level is increasing when the L/G ratio goes up for the two single-amine solvents. Furthermore, the sustainable-preferred packing type is as follows: Sulzer BX > Mellapak 250 Y > Mellapak plus 252Y > Flexipac 2Y.

A conclusion can be made that only the maximum L/G ratio of DIPA cases can satisfy the IMO 2050 carbon reduction strategy, and when the L/G ratio equals 1, DIPA solvent is not even eligible for the 2030 IMO carbon reduction plan. When L/G ratio exceeds 2, the MEA solvent can meet the IMO long-term strategy well, but not when the L/G ratio falls below 2.

In Fig. 7, the DIPA solution saves more energy than MEA, and when the L/G ratio goes up, more energy will be saved by adopting DIPA over MEA. From the perspective of energy saving, the preferred packing type would correspond to the highest carbon capture efficiency in most cases. The best energy-saving performance is 3.22 MJ/Kg CO_2 which is obtained by DIPA solvent with BX under L/G = 1, while the worst case is the MEA solvent with MEA with Flexipac 2Y under L/G = 4, which yields a value of 10.7 MJ/Kg CO_2.

To summarize, there will be a tradeoff between carbon capture performance and specific reboiler duty for the two single amines. Although DIPA is applicable for short-term IMO strategy with less energy consumption when the L/G ratio exceeds 2, MEA is recommended for most cases since its carbon capture performance is much better than that of DIPA.

Next, the TTPPCC process was conducted by introducing the blended MDEA and PZ solvent. The carbon capture performance and the specific reboiler duty of the three solvents are shown in Fig. 8.

Overall, the CO_2 capture efficiency of MDEA-PZ tops the other options, and its regeneration energy is between MEA and DIPA (see Fig. 8 (a)). When the liquid flow is equal to gas flow (L/G = 1 cases), the MDEA-PZ is still capable of meeting the 2050 IMO carbon strategy with the only exception being the Flexipac 2Y case. As for L/G = 2, all the blend amine cases generated great carbon capture results, as more than 95 % CO_2 from the ship engine flue gas was reduced by installing the TTPPCC system. DIPA is the best option for specific reboiler duty, and the blend-amine option presented performance similar to DIPA for the L/G = 1 cases; when the *leanin* flow rate is twice of that of the flue gas, the MDEA-PZ option can save more than 10 % energy for every mole captured CO_2 compared to the benchmark solvent MEA.

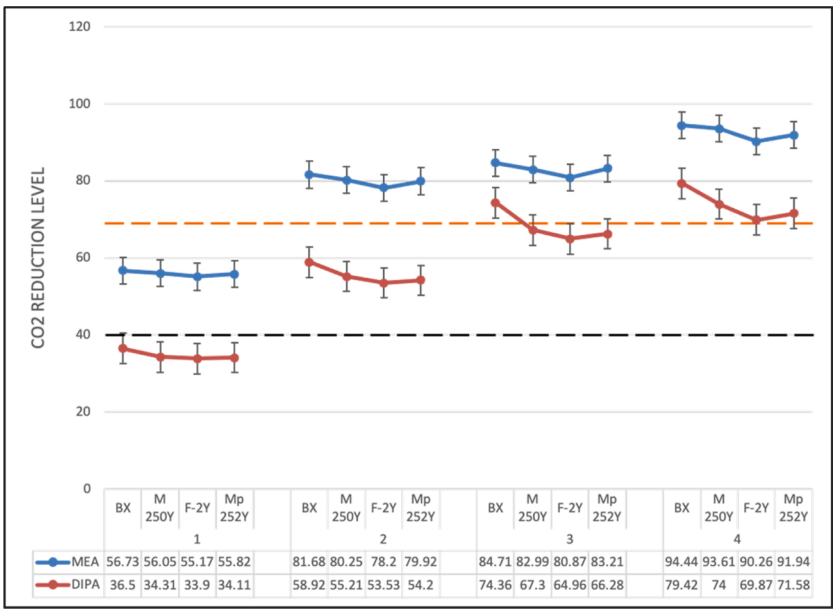

Fig. 6. CO_2 reduction efficiency of single amines: MEA and DIPA.

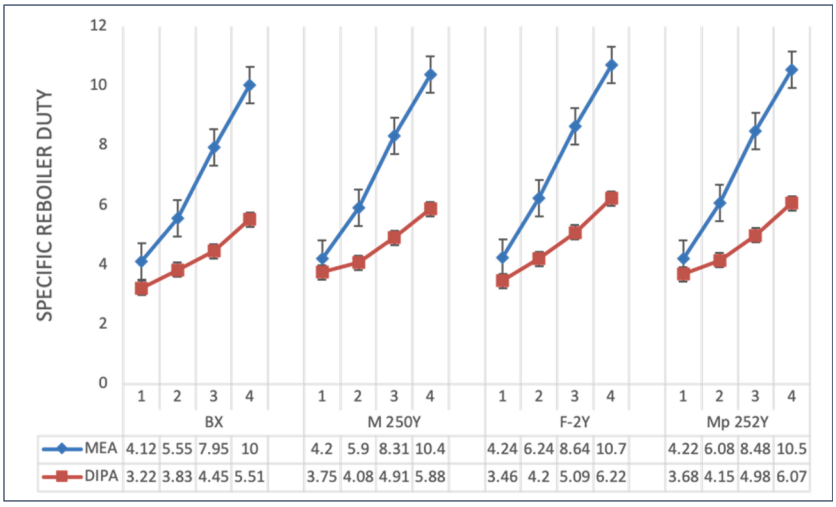

Fig. 7. Specific reboiler duty of MEA and DIPA.

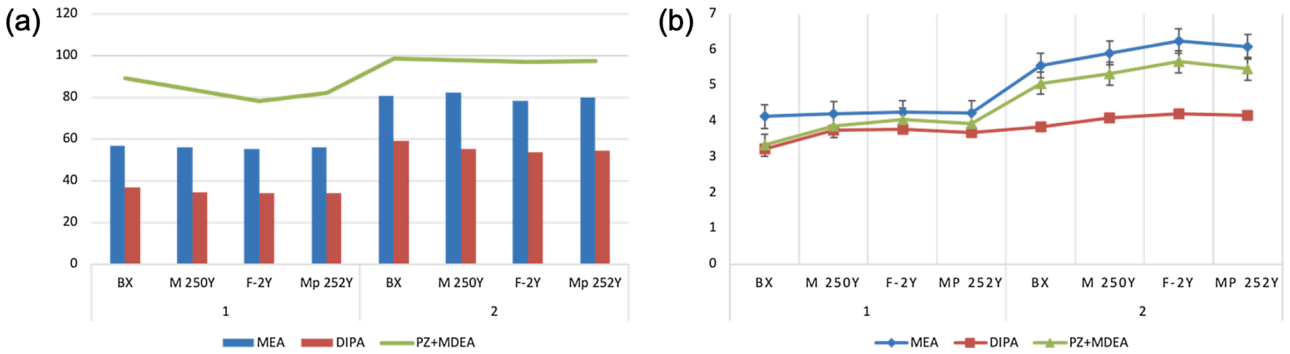

Fig. 8. (a) Carbon capture efficiency of MEA, DIPA and MDEA-PZ; (b) Specific reboiler duty of MEA, DIPA and MDEA-PZ.

Lastly, Fig. 9 illustrates the cyclic capacity of the three solvents, and the detailed calculated results are listed in Tab.S-5 of the supplemental document. The cyclic capacity has an inverse relationship with the lean solution flow rate, which can be reasonably predicted by the smaller holding time in the absorber led by the larger liquid flow rate, resulting in insufficient CO_2 absorbed by the selected solvents. The MDEA-PZ option exhibits superior cyclic capacity performance based on our process model, and the Sulzer BX with a lower liquid flow rate is

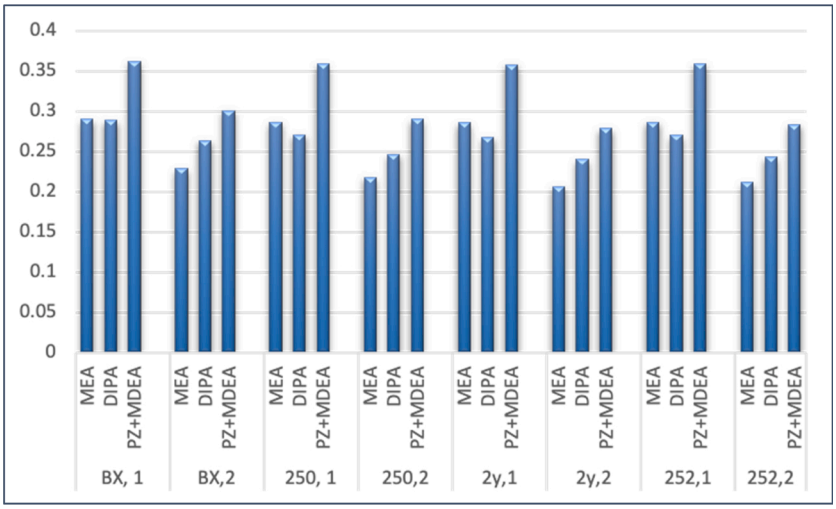

Fig. 9. Cyclic capacity of MEA, DIPA and MDEA-PZ.

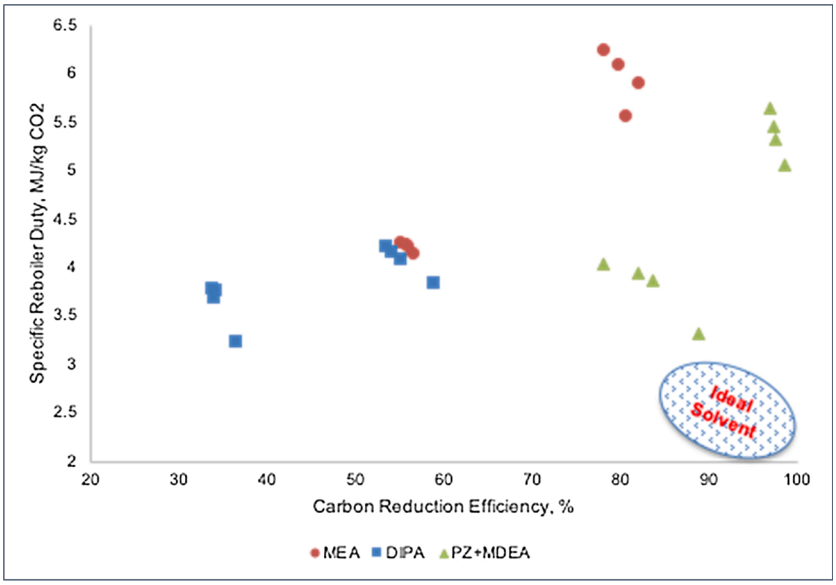

Fig. 10. CO_2 emission control and energy penalty tradeoff analysis of MEA, DIPA and MDEA-PZ.

recommended to reach a high-level cyclic capacity.

In summary, although a large carbon capture rate can be achieved by increasing the L/G ratio, the associated energy penalty increase rate is even higher, probably due to the inverse relationship between the liquid-gas ratio and the chemical absorption cyclic capacity. The ideal solvent for the TTPPCC system can be identified as low specific reboiler duty and high carbon reduction efficiency, as shown in the right corner of Fig. 10. Additionally, one can easily conclude that the cases of MDEA-PZ solvent with L/G equals to one have the best overall emission control-energy saving performance, and the MEA (L/G = 1) group and DIPA (L/G = 2) group share similar TTPPCC performance.

5. Conclusion

This study successfully established the process model of a 2-stroke ship engine system consisting of three Wärtsilä 12V50DF and one 6L50DF and presented a good validation result. Following the stages of sustainable process intensification, a rate-based aqueous MEA process model was developed and validated, then scaled up and modified to capture CO_2 from the flue gas. Also, a blended amine process model was established to simulate the onboard PCC system for the first time. The innovative design covered the absorber /stripper design with variation of solvents, packed type, and liquid gas ratio. A thorough sustainability evaluation of emission reduction efficiency, energy penalty, and carbon cyclic capacity was conducted among three aqueous amine options: MEA, DIPA, and MDEA-PZ. Compared to the benchmark aqueous amine MEA, the MDEA-PZ option could capture more than 57 % CO_2 while around 25 % specific reboiler duty can be saved. The generated results confirmed that the Sulzer BX was preferred among the selected four packing types from the perspective of carbon capture efficiency and energy requirement for solvent regeneration, and the cyclic capacity has an inverse relationship with the lean solution flow rate.

Newly blended aqueous amines, particularly ternary mixtures, might be the next focus on the solvent selection of the chemical absorption-based maritime capture system, despite the binary blended amines displaying satisfactory PCC performance in this study. The TTPPCC system needs more studies on the kinetics modeling, the second-order absorption rate constant, and activation energy to meet its requirement of fast reaction rate and low energy consumption. Moreover, process design for intensified unit operations involving rotating packed bed and printed

circuit heat exchangers is another direction to expand on this study. Other post-combustion carbon capture techniques such as membrane-based approach, adsorption, and physical absorption can be integrated to the TTPPCC system as well.

Author statement

Chenxi Ji: Investigation, Data Curation, Model Development, Formal Analysis, Writing-Original Draft.

Shuai Yuan: Methodology, Visualization, Model validation.

Mitchell Huffman: Validation, Writing-Review & Editing.

Mahmoud M. El-Halwagi: Process Analysis, Supervision, Writing-Review & Editing.

Qingsheng Wang: Project Administration, Supervision, Writing-Review & Editing.

Declaration of Competing Interest

The authors report no declarations of interest.

Appendix A. Supplementary data

Supplementary material related to this article can be found, in the online version, at doi:https://doi.org/10.1016/j.jcou.2021.101655.

References

[1] I. MEPC 72, Initial IMO Strategy on Reduction of GHG Emissions from Ships, 304, 2018, pp. 1–11.

[2] Argonne National Laboratory, The Greenhouse Gases, Regulated Emissions, and Energy Use in Transportation (GREET) Model, (n.d.). http://greet.es.anl.gov/.

[3] F. Baldi, S. Bengtsson, K. Andersson, The influence of propulsion system design on the carbon footprint of different marine fuels, Low Carbon Shipp. Conf. (2013).

[4] I. Baresic, D. Smith, T. Raucci, C. Rehmatulla, N. Narula, K. Rojon, LNG As a Marine Fuel in the EU. Market, Bunkering Infrastructure Investments and Risks in the Context of GHG Reductions, 2019 https://sea-lng.org/wp-content/uploads/2019/01/190123_SEALNG_InvestmentCase_DESIGN_FINAL.pdf%0A https://sea-lng.org/independent-study-reveals-compelling-investment-case-for-lng-as-a-marine-fuel/.

[5] S. Bengtsson, E. Fridell, K. Andersson, Environmental assessment of two pathways towards the use of biofuels in shipping, Energy Policy 44 (2012) 451–463, https://doi.org/10.1016/j.enpol.2012.02.030.

[6] H.M. El-Houjeiri, A.R. Brandt, J.E. Duffy, Open-source LCA tool for estimating greenhouse gas emissions from crude oil production using field characteristics, Environ. Sci. Technol. (2013), https://doi.org/10.1021/es304570m.

[7] H. El-Houjeiri, J.C. Monfort, J. Bouchard, S. Przesmitzki, Life cycle assessment of greenhouse gas emissions from marine fuels: a case study of saudi crude oil versus natural gas in different global regions, J. Ind. Ecol. 23 (2019) 374–388, https://doi.org/10.1111/jiec.12751.

[8] P. Gilbert, C. Walsh, M. Traut, U. Kesieme, K. Pazouki, A. Murphy, Assessment of full life-cycle air emissions of alternative shipping fuels, J. Clean. Prod. 172 (2018) 855–866, https://doi.org/10.1016/j.jclepro.2017.10.165.

[9] J.L. Manganaro, A. Lawal, CO2 life-cycle assessment of the production of algae-based liquid fuel compared to crude oil to diesel, Energy Fuels (2016), https://doi.org/10.1021/acs.energyfuels.6b00207.

[10] F. Verbeek, Ruud Kadijk, Gerrit Mensch, Pim van Wulffers, Chris Beemt, Bas van den Fraga, Environmental and Economic Aspects of Using LNG as a Fuel for Shipping in the Netherlands, 2011.

[11] F. Baldi, T. Van Nguyen, F. Ahlgren, The application of process integration to the optimisation of cruise ship energy systems: a case study, ECOS 2016 - Proc.29th Int. Conf. Effic. Cost, Optimisation, Simul. Environ. Impact Energy Syst. (2016).

[12] F. Baldi, F. Ahlgren, T. Van Nguyen, M. Thern, K. Andersson, Energy and exergy analysis of a cruise ship, Energies 11 (2018) 1–41, https://doi.org/10.3390/en11102508.

[13] C. Ji, S. Yuan, Z. Jiao, M. Huffman, M.M. El-Halwagi, Q. Wang, Predicting flammability-leading properties for liquid aerosol safety via machine learning, Process Saf. Environ. Prot. 148 (2021) 1357–1366, https://doi.org/10.1016/j.psep.2021.03.012.

[14] C. Ji, Z. Jiao, S. Yuan, M.M. El-Halwagi, Q. Wang, Development of novel combustion risk index for flammable liquids based on unsupervised clustering algorithms, J. Loss Prev. Process Ind. (2021), https://doi.org/10.1016/j.jlp.2021.104422.

[15] X. Luo, M. Wang, Study of solvent-based carbon capture for cargo ships through process modelling and simulation, Appl. Energy 195 (2017) 402–413, https://doi.org/10.1016/j.apenergy.2017.03.027.

[16] M. Feenstra, J. Monteiro, J.T. van den Akker, M.R.M. Abu-Zahra, E. Gilling, E. Goetheer, Ship-based carbon capture onboard of diesel or LNG-fuelled ships, Int. J. Greenh. Gas Control. 85 (2019) 1–10, https://doi.org/10.1016/j.ijggc.2019.03.008.

[17] G. Shu, Y. Liang, H. Wei, H. Tian, J. Zhao, L. Liu, A review of waste heat recovery on two-stroke IC engine aboard ships, Renewable Sustainable Energy Rev. 19 (2013) 385–401, https://doi.org/10.1016/j.rser.2012.11.034.

[18] M.H. Yang, R.H. Yeh, Thermodynamic and economic performances optimization of an organic Rankine cycle system utilizing exhaust gas of a large marine diesel engine, Appl. Energy 149 (2015) 1–12, https://doi.org/10.1016/j.apenergy.2015.03.083.

[19] P. DNV, Ship Carbon Capture and Storage, 2013.

[20] A. Awoyomi, K. Patchigolla, E.J. Anthony, CO2/SO2 emission reduction in CO2 shipping infrastructure, Int. J. Greenh. Gas Control. 88 (2019) 57–70, https://doi.org/10.1016/j.ijggc.2019.05.011.

[21] A. Van De Haar, C. Trapp, K. Wellner, R. De Kler, G. Schmitz, P. Colonna, Dynamics of postcombustion CO2 capture plants: modeling, validation, and case study, Ind. Eng. Chem. Res. 56 (2017) 1810–1822, https://doi.org/10.1021/acs.iecr.6b00034.

[22] C. Ji, M.M. El-Halwagi, A data-driven study of IMO compliant fuel emissions with consideration of black carbon aerosols, Ocean Eng. 218 (2020), https://doi.org/10.1016/j.oceaneng.2020.108241, 108241.

[23] Wärtsilä, Wärtsilä 50DF Product Guide, 2019.

[24] Q. Xie, Simulation of Combustion Characteristics in a LNG/diesel Dual Fuel Engine, Wuhan University of Technology, 2017.

[25] Aspen Technology, Aspen Physical Property System Physical Property Methods and Models, 2006. http://www.aspentech.com.

[26] S.W. Brelvi, J.P. O'Connell, Corresponding states correlations for liquid compressibility and partial molal volumes of gases at infinite dilution in liquids, AIChE J. (1972), https://doi.org/10.1002/aic.690180622.

[27] Y. Yan, C.C. Chen, Thermodynamic modeling of CO2 solubility in aqueous solutions of NaCl and Na2SO4, J. Supercrit. Fluids (2010), https://doi.org/10.1016/j.supflu.2010.09.039.

[28] Y. Liu, L. Zhang, S. Watanasiri, Representing vapor-liquid equilibrium for an aqueous MEA-CO2 system using the electrolyte nonrandom-two-liquid model, Ind. Eng. Chem. Res. (1999), https://doi.org/10.1021/ie980600v.

[29] Aspen Technology Inc, Aspen Physical Property System, 2019 version 11.

[30] Y. Zhang, H. Que, C.C. Chen, Thermodynamic modeling for CO2 absorption in aqueous MEA solution with electrolyte NRTL model, Fluid Phase Equilib. (2011), https://doi.org/10.1016/j.fluid.2011.08.025.

[31] R. Notz, H.P. Mangalapally, H. Hasse, Post combustion CO2 capture by reactive absorption: pilot plant description and results of systematic studies with MEA, Int. J. Greenh. Gas Control. 6 (2012) 84–112, https://doi.org/10.1016/j.ijggc.2011.11.004.

[32] J.L. Bravo, J.A. Rocha, J.R. Fair, Mass transfer in gauze packings, Hydrocarb. Process. (1985).

[33] D.K. Babi, P. Lutze, J.M. Woodley, R. Gani, A process synthesis-intensification framework for the development of sustainable membrane-based operations, Chem. Eng. Process. Process Intensif. 86 (2014) 173–195, https://doi.org/10.1016/j.cep.2014.07.001.

[34] E.O. Agbonghae, K.J. Hughes, D.B. Ingham, L. Ma, M. Pourkashanian, Optimal process design of commercial-scale amine-based CO2 capture plants, Ind. Eng. Chem. Res. 53 (2014) 14815–14829, https://doi.org/10.1021/ie5023767.

[35] J.G. Stichlmair, J.R. Fair, Distillation: Principles and Practices, 1998.

[36] G. Towler, R.K. Sinnott, Chemical Engineering Design - Principles, Practice and Economics of Plant and Process Design, 2nd edition, 2013.

[37] A. Haghtalab, H. Eghbali, A. Shojaeian, Experiment and modeling solubility of CO2 in aqueous solutions of Diisopropanolamine + 2-amino-2-methyl-1-propanol + Piperazine at high pressures, J. Chem. Thermodyn. 71 (2014) 71–83, https://doi.org/10.1016/j.jct.2013.11.025.

[38] Z. Liang, W. Rongwong, H. Liu, K. Fu, H. Gao, F. Cao, R. Zhang, T. Sema, A. Henni, K. Sumon, D. Nath, D. Gelowitz, W. Srisang, C. Saiwan, A. Benamor, M. Al-Marri, H. Shi, T. Supap, C. Chan, Q. Zhou, M. Abu-Zahra, M. Wilson, W. Olson, R. Idem, P. P.T. Tontiwachwuthikul, Recent progress and new developments in post-combustion carbon-capture technology with amine based solvents, Int. J. Greenh. Gas Control. 40 (2015) 26–54, https://doi.org/10.1016/j.ijggc.2015.06.017.